Article

Glaucoma Detection Based on Texture Feature of Neuro Retinal Rim Area in Retinal Fundus Image

Gibran Satya Nugraha [1*], Akbar Juliansyah [2] and Muhammad Tajuddin [2]

[1] Department of Informatics Engineering, University of Mataram; gibransn@unram.ac.id
[2] Department of Computer Science; Bumigora University; akbarjuliansyahstmmt@gmail.com, tajuddin@universitasbumigora.ac.id

* Correspondence: gibransn@unram.ac.id

Abstract: One method for detecting glaucoma is by comparing ratios in the area of neuroretinal rim. Comparing area ratios in the neuroretinal rim is difficult for ophthalmologists since it requires high accuracy and is highly dependent on the patient's retinal condition. In this study, we sought to perform neuro retinal rim feature extraction based on histogram and gray level co-occurrence matrix (GLCM) of normal retinal images and glaucoma, automatically distinguish between normal eyes and eyes with glaucoma, and evaluate the method's validity using the measures of accuracy, sensitivity, and specificity We adopted a machine learning approach in conducting automatic feature extraction of the retinal rim through three main stages: 1) image acquisition, 2) pre-processing, and 3) classification. We used a dataset from RIM-ONE for normal eyes images and DRISTHI-GS for glaucoma images.Classification was carried out on 154 images (80 images for glaucoma images and 74 images for normal images). Regarding true positive, false negative, false positive, and true negative, we examined the sensitivity, specificity, and accuracy of automatic extraction and classification. The highest findings are 96.10%, 98.75%, and 93.24%, respectively.
This study showed that automatic texture features and classification are possible, accurate and important in detecting glaucoma.

Keywords: glaucoma; classification; biomedicine; machine learning; neuro retinal rim

Citation: G. S. Nugraha, A. Juliansyah, and M. Tajuddin, "Glaucoma Detection Based on Texture Feature of Neuro Retinal Rim Area in Retinal Fundus Image", *IJHIS*, vol. 1, no. 3, pp. 106–116, Jan. 2024.

Received: 20-09-2023
Revised: 22-12-2023
Accepted: 30-12-2023
Published: 03-01-2024

1. Introduction

Glaucoma is a disease that attacks retina of the eye and progresses gradually over lifetime. This disease is difficult to detect early and often detected when it has reached high level of severity [1]. Glaucoma damages the optic nerve tissue in the eye, raises intraocular pressure, impairs vision, and eventually results in blindness [2]. Blindness caused by glaucoma is difficult to treat, therefore, early detection of glaucoma is critical [3]. There is a glaucoma detection technique that is extremely common. Comparing the ISNT (inferior, superior, nasal, and temporal) areas [4], is one such example, as seen in Figure 1. Normal eyes have an order of area according to the ISNT rule. If something doesn't match the order, then the eye is diagnosed with glaucoma [5] [6]. Comparing the area ratios in the neuro retinal rim, however, is difficulty for ophthalmologist to do manually, since it requires high accuracy and highly dependence on patient's retinal condition. Thus, automatic feature extraction of retinal image provides a rapid and accurate solution to detect glaucoma.

The research on feature extraction to classify normal and abnormal images of a retina has been conducted globally, but limited studies have done it in the context of glaucoma detection. Harini et al. extracted features on 75 normal images and those affected by diabetic retinopathy. 45 images (9 normal, 36 diabetic retinopathy) were used as data training and 30 images (6 normal, 24 diabetic retinopathy) as data testing. The classifier used is Support Vector Machine. The results obtained are accuracy of 96.67%, sensitivity

of 100% and specificity of 95.83%. Pre-processing was performed prior to the feature extraction stage, which consists of contrast enhancement and morphological operations [7]. Dong et al. classified normal images and those affected by cataract using deep learning. The features taken have a maximum entropy with the accuracy of 84.7% [8]. Choudhury classifies normal images and those affected by diabetic retinopathy. The features used are exudates and vessel density, which are extracted using fuzzy c-means to then be classified using a support vector machine resulting in 97.6% of accuracy [9]. From these previous research, automatic feature extraction on retinal images is feasible and yielded high accuracy results. Furthermore, feature extraction can overcome the weakness of the dataset, for example if the image has a resolution that is not too good, with machine learning that is done automatically, the image can still be diagnosed as normal or glaucoma.

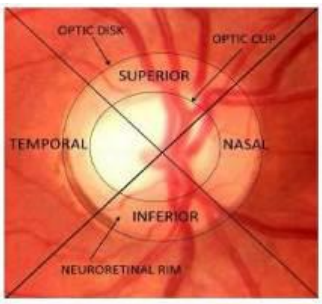

Figure 1. Retinal fundus image [4]

We previously did research on the automatic segmentation of the neural retinal rim area, and we put out a strategy for doing so based on histogram data (mean and standard deviation) [10]. It was discovered that 73 out of 80 retinal pictures with glaucoma from the DRISTHI-GS databases [11] had the disease correctly identified. As a result, the accuracy was 91.25% [10]. But, in order to more thoroughly verify this method's dependability, we must increase the number of datasets and look into how adaptable it is to various dataset settings.

In this study, we aimed to feature extract from normal retinal images and glaucoma images using histogram and gray level co-occurrence matrix (GLCM) of normal retinal images and glaucoma, automatically classified normal eyes versus eyes with glaucoma, and assessed the validity of the method through the measure of accuracy, sensitivity, and specificity.

2. Materials and Methods

This research consists of three main stages, namely image acquisition, pre-processing, and classification. This analysis was conducted using Matlab R2010a.

2.1 Image Acquisition

This research uses a retinal image dataset from RIM-ONE [12] for normal images and DRISTHI-GS for glaucoma images [11], both retinal image datasets are publicly available, therefor ethics approval is not required for this study. Figure 2 (a) displays RIM-ONE image examples, while Figure 2 (b) displays DRISTHI-GS image examples. (b). RIM-ONE is a normal retinal image containing 74 JPG images, while DRISTHI-GS is a glaucoma-affected retinal image with 80 PNG photos. The capture of images is the initial step in this study procedure. Figure 3 shows information on how the segmentation and classification process is carried out. Some of the main points here are extracting the red component in the image because the red component significantly shows the difference between the object and the background, then carrying out contrast enhancement and segmentation of the

optic cup and optic disc. The final step is to obtain the neuroretinal rim area, and then classify the features that have been extracted.

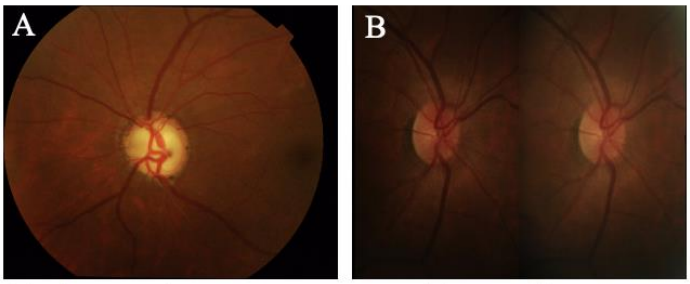

Figure 2. (a) Glaucoma image DRISTHI-GS, (b) normal image RIM-ONE

2.2 Pre-processing

The retinal fundus image is an RGB image. As processing images with three color components at once will take a long time, choosing one color component that can facilitate segmentation needs to be done. Based on experiments conducted, the red component is able to distinguish between the disc and the retina. Therefore, we converted the image color to red and conducted contrast enhancement. Contrast enhancement is needed so that the histogram values become more uniform, making it easier to segment the disc. One of the contrast enhancement methods is contrast stretching. This method distributes the gray level evenly [13]. Once the contrast stretching is done, we conducted image cropping. Cropping is a method used to improve the quality of the image taken and also to focus on a particular area of object to be observed. In addition, cropping also aims to change the composition of the image and its ratio [14]. In this research, dimension of the cropping result is 500x500.

Since the optic disc and optic cup in Figure 4(a) and (b) are white, a threshold value computed from pixel intensity between 200 and 250 is necessary to separate or segment the optic disc and optic cup from the remainder of the retina. We generated this threshold value by computing the mean and standard deviation of the image's histogram.

Mean is one of the parameters of the histogram, which shows the average of the, which can be calculated with Equation (1). The standard deviation measures the closeness of the data to their mean, which can be calculated with Equation (2). Threshold values for optical disc and optic cup segmentation are obtained from Equations (3) and (4) respectively [15][16]. The constant "4" in Equation (4) is determined by observing and analyzing the optical cup segmentation of all images utilized in this investigation. After the segmentation method has been finished, morphology can be used to eradicate any blood vessels that remain in the optical cup or optical disc. [10].

$$m = \sum_{i=0}^{L=1} i.p(i) \tag{1}$$

$$\sigma = \sqrt{\sum_{i=1}^{L-1} (i-m)^2 \, p(i)} \tag{2}$$

$$disc = mean + stdev \tag{3}$$

$$cup = mean + 4 * stdev \tag{4}$$

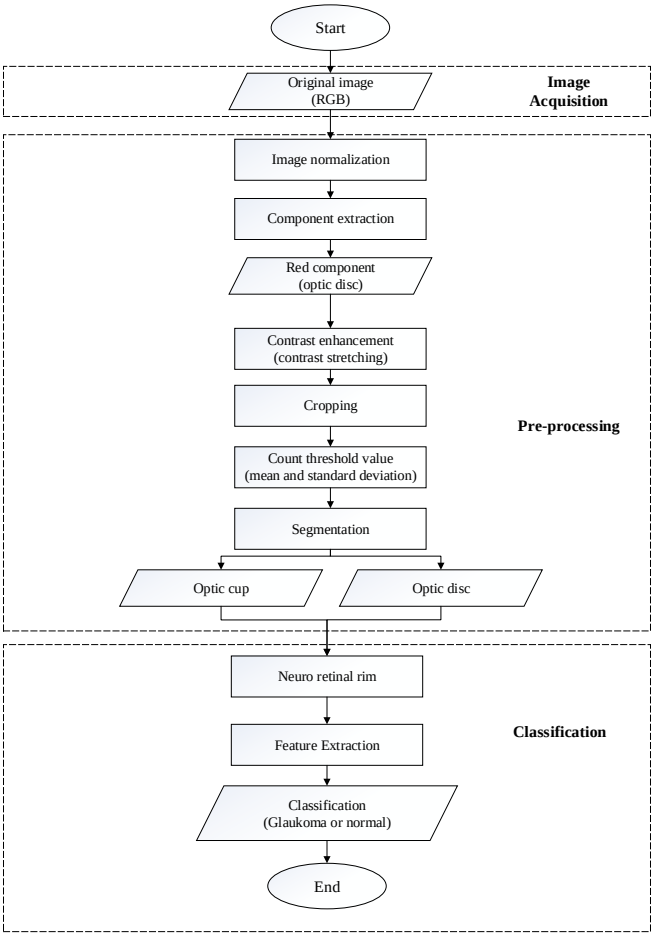

Figure 3. Three main research stages: acquisition, pre-processing, and classification

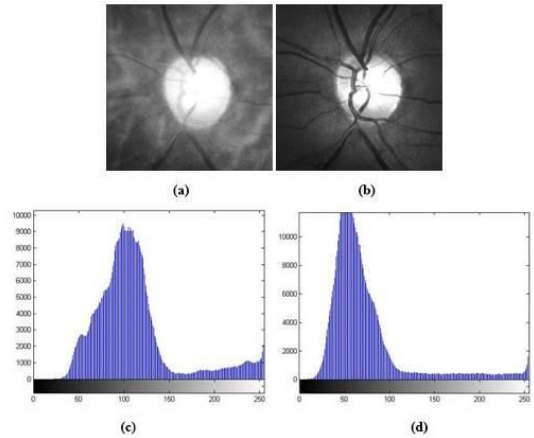

Figure 4. Histogram result from cropping image, (a) optic disc, (b) optic cup, (c) histogram optic disc, (d) histogram optic cup

2.3 Feature Extraction

The features or characteristics referred to are values that can be parameters of the characteristics of an image. These features will be used to differentiate between one object and another and divide these objects according to their respective classes. In this research, we used two different classifications, which are "glaucoma" and "normal". In addition to GLCM features, which are composed of five different components: angular second moment (ASM), contrast, inverse different moment (IDM), entropy, and correlation, the

texture-based histogram used for feature extraction uses six different components: mean, standard deviation, skewness, energy, entropy, and smoothness.

The mean of intensity is the first characteristic that is statistically calculated. Based on the Equation (5), this feature's components are determined.

$$m = \sum_{i=0}^{L-1} i \, . p(i) \tag{5}$$

In this instance, the grey level i represents the likelihood that the color i will appear in the images f and $p(i)$, respectively, and the maximum grey level L. The average brightness of the item will be calculated using the algorithm above. A standard deviation is the second attribute. Equation 6 has the following calculations.

$$\sigma = \sqrt{\sum_{i=1}^{L-1} (i-m)^2 p(i)} \tag{6}$$

In this instance, as $p(i)$ is a function of opportunity, σ^2 is referred to as variance or normalized second-order moment. This characteristic offers some contrast. The skewness function is a measure of the skewness of the average intensity value. Definition of Equation (7):

$$skewness = \sum_{i=1}^{L-1} (i-m)^3 p(i) \tag{7}$$

Skewness is often referred to as the cubic normalized moment. Negative values indicate that the luminance distribution is shifting to the left toward the mean value, while positive values indicate that the luminance distribution is shifting to the right toward the mean value. It is normalized because its divide the skewness value by $(L\text{-}1)^2$. Measurements that convey the distribution of pixel intensity over the grayscale are called energy descriptors. Equation (8) gives the following definition:

$$energy = \sum_{i=0}^{L-1} [p(i)]^2 \tag{8}$$

The highest energy value of a homogeneous grayscale image is 1. Images with fewer gray levels typically have more energy than pictures with more gray levels. Uniformity is another name for energy. Entropy is a measure of how complex an image is. Equation (9)'s calculation is as follows:

$$entropy = -\sum_{i=0}^{L-1} p(i) \, \log_2(p(i)) \tag{9}$$

The complexity of the image will increase with the entropy value. Remember that entropy and energy are usually polar opposites. The quantity of information present in the data distribution is also represented by entropy. The smoothness feature is typically provided to quantify the smoothness or roughness of an image's intensity. The definition is given in Equation 10 as follows:

In the formula above, σ is the standard deviation. Based on the formula above, a low R value indicates that the image has a rough intensity. Please be aware that the variance

must be normalized before calculating the smoothness. By dividing the value by $(L-1)^2$, we can see that it falls between 0 and 1.

Second-order texture calculations are used by GLCM. When measuring textures in the first order using statistical computations, the neighbor pixel relationship is not taken into consideration and instead is dependent on the pixel value of the original image, such as variance. In the second order, the relationship between pairs of two original images is considered.

The following procedure in Equation (10) is used to determine ASM, a measure of image uniformity. In this instance, L stands for the quantity of computing levels. Equation (11) uses the following approach to determine contrast, which is a measurement of the existence of differences in the gray level of the picture pixel. IDM is utilized to determine homogeneity. In Equation (12), IDM is determined using the following method. Entropy quantifies the size of gray level variations in an image. If the GLCM component values are close to one another, then the value is high. The value is low if the values of the GLCM elements are near to 0 or 1. The formula for calculating entropy can be found in Equation (13). The formula in Equation (14) is utilized to determine the correlation, which is a measure of linear dependence between gray levels in an image.

$$ASM = \sum_{i=1}^{L}\sum_{j=1}^{L}(GLCM(i,j)^2 \tag{10}$$

$$Contrast = \sum_{n=1}^{L} n^{2}\left\{\sum_{|i-j|=n} GLCM(i,j)\right\} \tag{11}$$

$$IDM = \sum_{i=1}^{L}\sum_{j=1}^{L}\frac{(GLCM(i,j)^2}{1+(i-j)^2} \tag{12}$$

$$Entropy = -\sum_{i=1}^{L}\sum_{j=1}^{L}(GLCM(i,j)\log(GLCM(i,j) \tag{13}$$

$$Correlation = \frac{\sum_{i=1}^{L}\sum_{j=1}^{L}(ij)(GLCM(i,j)-\mu_i{}'\mu_j{}'}{\sigma_i{}'\sigma_j{}'} \tag{14}$$

2.4 Classification

The final stage of this research is the classification which aims to classify the images used into normal or glaucoma classes, where in the series of previous stages, various processes have been carried out to obtain a number of features that represent both normal and glaucoma images. The values of these features were trained with the Multi-Layer Perceptron algorithm with the back-error propagation learning method to obtain weight values that could be used in testing the data to be classified next. The testing stage in this research used the k-fold cross validation technique. Cross validation aims to classify the number of data as a given fold. Thus, each data can certainly be training data and testing data.

3. Results and Discussion

3.1 Pre-processing

As demonstrated in Figure 5.A.1, the red component distinguishes the optical disc from the remainder of the retina. Therefore, the red component is extracted in order to process the optical disc and optical cup. As depicted in Figure 5.B, the contrast enhancement technique adopted is contrast stretching since it provides a reasonably clear image for the retina. Figure 5.C illustrates the results of cropping the image with the center of the brightest portion of the retina image on the 500x500 optical disc.

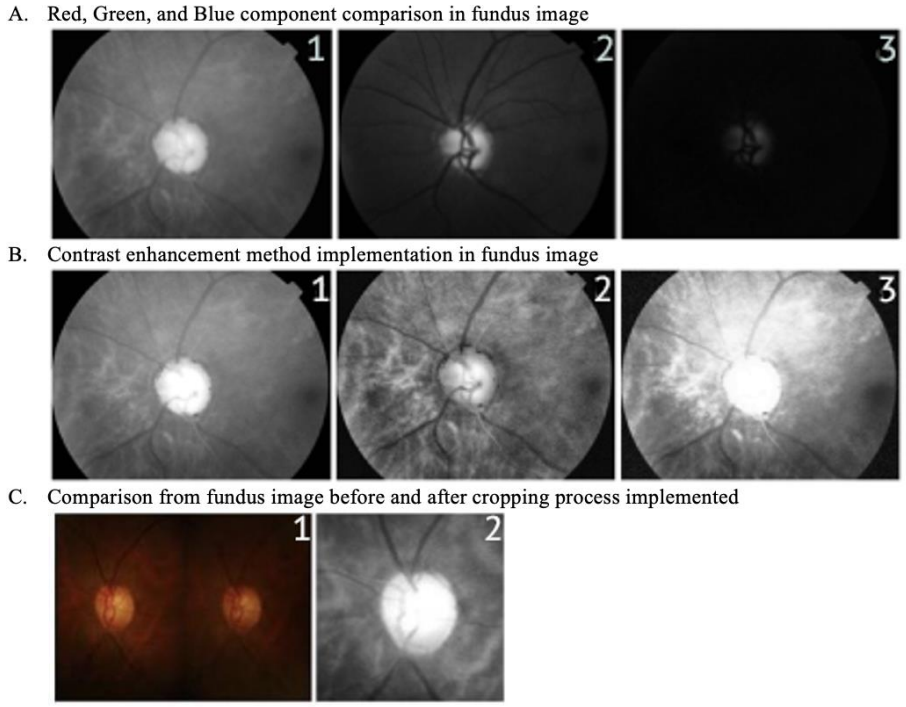

Figure 5. (A.1) Red component, (A.2) Green component, (A.3) Blue component, (B.1) Contrast stretching, (B.2) Histogram Equalization, (B.3) CLAHE, (C.1) Original results, (C.2) Cropping result

3.2 Segmentation

The results of optical disc segmentation, optical cup analysis, and neural retinal rim area analysis are depicted in Figure 6. Using an optical cup to separate the optical disc, the neural retinal rim was obtained. In addition, the histogram and GLCM features were utilized to extract the neuronal retinal rim portion.

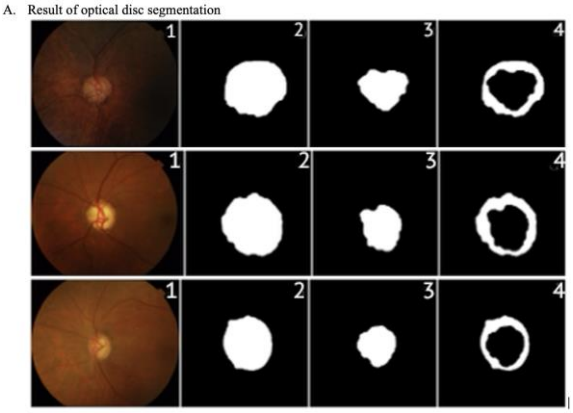

Figure 6. (A.1) Retinal fundus image, (A.2) segmentation of optic disc, (A.3) segmentation of optic cup, (A.4) segmentation of neuro retinal rim.

3.3 Feature Extraction

Table 1. Histogram result for glaucoma image

Img	Mean	Standard deviation	Skewness	Energy	Entropy (histogram)	Smooth-ness	Class
1	89.982	120.903	16.693	0.456	1.237	0.184	Glaucoma
2	85.738	119.306	18.047	0.456	1.301	0.180	Glaucoma
3	86.684	120.237	18.011	0.460	1.187	0.182	Glaucoma
4	81.172	118.287	19.822	0.480	1.125	0.177	Glaucoma
5	136.623	126.744	-4.537	0.423	1.165	0.198	Glaucoma

Table 2. GLCM result for glaucoma image

Image	ASM	Contrast	IDM	Entropy (GLCM)	Correlation	Class
1	0.414	453.584	0.890	1.753	0.0000670	Glaucoma
2	0.415	439.260	0.879	1.852	0.0000690	Glaucoma
3	0.406	689.864	0.877	1.736	0.0000670	Glaucoma
4	0.429	652.046	0.890	1.626	0.0000700	Glaucoma
5	0.377	569.950	0.899	1.631	0.0000610	Glaucoma

In Table 1 the mean value is more than 80, this shows that the pixel intensity of the glaucoma image is quite high, but for normal images as shown in Table 2 the mean value is very small, which indicates the pixel intensity is low. The standard deviation feature value in glaucoma images is also higher than normal images, can be seen in Tables 1 and Table 2. The standard deviation indicates the magnitude of an object's contrast value. This demonstrates that the glaucoma image has a higher contrast value than the normal image. Other characteristics, such as skewness, indicate that if the value is positive, the brightness distribution is skewed to the right toward the mean, and vice versa if the value is negative. Tables 1 and 2 reveal that the majority of skewness values for glaucoma and normal pictures are positive.

Table 3. Histogram result for normal image

Img	Mean	Standard deviation	Skewness	Energy	Entropy (histogram)	Smooth -ness	Class
6	19.219	67.165	14.991	0.848	0.360	0.065	normal
7	38.422	91.110	22.716	0.732	0.520	0.113	normal
8	20.052	68.511	15.483	0.844	0.358	0.067	normal
9	21.914	71.354	16.508	0.833	0.371	0.073	normal
10	27.954	79.546	19.344	0.793	0.437	0.089	normal

Table 4. GLCM feature result for normal image

Image	ASM	Contrast	IDM	Entropy (GLCM)	Correlation	Class
6	0.840	139.833	0.982	0.449	0.0002170	normal
7	0.723	135.349	0.982	0.612	0.0001190	normal

Image	ASM	Contrast	IDM	Entropy (GLCM)	Correlation	Class
8	0.836	127.544	0.984	0.439	0.0002090	normal
9	0.825	121.327	0.985	0.448	0.0001930	normal
10	0.785	126.476	0.983	0.523	0.0001560	normal

The fourth characteristic of the histogram is energy, which is near to 1 if the image has a uniform gray level. Normal and glaucoma images exhibit highly varying energy values; in glaucoma photos, the energy value is typically less than 0.5, but in normal images, it is near to 1. This means that the normal image has a gray level that is pretty homogeneous. The entropy value is the inverse of the energy value. The greater the value of entropy, the more complicated the image. Seen in Tables 1 and 2, the entropy value of glaucoma images is higher than normal images. This shows that glaucoma images have a higher complexity than normal images. The smoothness value in the image shows the level of smoothness of the intensity in the image. The lower the smoothness value, the coarser the intensity of the image. Tables 1 and 2 show that the smoothness values for normal and glaucoma images are quite similar.

The ASM value indicates image homogeneity for the GLCM feature; the greater the ASM value, the more homogeneous the image intensity. The ASM values for glaucoma and normal images are comparable in Tables 3 and 4. A high contrast value means that an image has a high level of gray level variation. In Table 3 the contrast value of glaucoma images is higher than normal images (Table 4). This shows that glaucoma images have more varied levels of gray than normal images. While the correlation value is a value that shows a linear dependence between levels of gray in the image. The higher the correlation value, the higher the linear dependence. Tables 3 and 4 which assess the correlation of glaucoma and normal images show that the correlation values of the 2 categories of images are relatively the same.

The values of all features (histogram and GLCM) will be used as input to the classifier. There is no value that truly reflects a normal or glaucoma image, so a classification is needed in order to distinguish between normal and glaucoma images.

3.4 Classification

Classification was carried out on 154 images used in this research. We measured the classification accuracy, sensitivity, and specificity that refer to true positive (TP), false negative (FN), false positive (FP), and true negative (TN). The results of the can be seen in Table 5. From the table, we can see that this method has yielded the highest accuracy, sensitivity and specificity values of 96.10%, 98.75% and 93.24%, respectively.

Table 5. Classification results

Feature	TP	FN	FP	TN	Accuracy	Sensitivity	Specificity
All	79	1	5	69	96.10	98.75	93.24

3.5 Discussion

The result of this study indicates that feature extraction is able to provide results of accuracy, sensitivity, and specificity whose values are above 93%. The results of this study further confirm that the feature extraction approach in diagnosing a disease can give good results, as evidenced by several similar studies with different eye diseases that have been described in the Introduction section.

To see how far the contribution of the research results that have been done. We compared the results of this study with other studies regarding glaucoma detection using different feature extractions and different machine learning methods, details of the comparison of the results can be seen in Table 6. The research we compare uses local datasets with varying number of datasets, features, and classifiers. We can see that our proposed method provides the same relative accuracy as other studies.

The advantage of this research is that although it uses conventional machine learning methods such as artificial neural networks, it can provide accuracy, sensitivity, and specificity above 93%. Histogram and GLCM features that we use here have a very big role in selecting features that represent glaucoma and normal images.

The segmentation stage of the disc and cup sections in this study is very important, because the disc and cup sections are the parts that will be separated to obtain the neuroretinal rim area. The segmentation method used is adaptive using a combination of the mean and standard deviation values of the image. Further experiments are needed on other datasets using this segmentation method to find the most adaptive model in segmenting disc and cup sections. Further research also needs to combine other features in the classification so that better accuracy is obtained and can also minimize computational time.

Future research can also try to detect glaucoma directly through the outer eye, not through retinal images. Such detection can be done in real time using a smartphone. Of course, research like this is a tremendous breakthrough in terms of research on glaucoma detection using machine learning techniques.

4. Conclusions

In this research, we are able to conduct automatic glaucoma detection based on texture features on the neuro retinal rim area. The dataset used are DRISTHI-GS, providing 80 glaucoma images, and RIM-ONE, which provide 74 normal images. The detection process starts with image acquisition process, followed by pre-processing, which include extracting the red component, cropping the image, and contrast enhancement. The next process the include extracting the histogram and GLCM features from neuro retinal rim area, which consisting of total eleven components: mean, standard deviation, skewness, energy, entropy, smoothness, ASM, contrast, inverse different moment IDM, entropy, and correlation. Testing phase uses k-fold cross validation, with 10 folds. The classification has yielded high value of accuracy, sensitivity, and specificity obtained were 93.38%, 95.45%, and 91.43% respectively. This study shows that automatic glaucoma detection using feature extraction is promising field to be explored by researchers and medical practitioners.

References

1. T. Khalil, M. U. Akram, H. Raja, A. Jameel, and I. Basit, "Detection of Glaucoma using Cup to Disc Ratio from Spectral Domain Optical Coherence Tomography Images," *IEEE Access*, vol. 6, pp. 4560–4576, 2018, doi: 10.1109/ACCESS.2018.2791427.
2. T. Khalil, M. U. Akram, S. Khalid, and A. Jameel, "Improved automated detection of glaucoma from fundus image using hybrid structural and textural features," *IET Image Process*, vol. 11, no. 9, pp. 693–700, 2017, doi: 10.1049/iet-ipr.2016.0812.
3. H. Fu *et al.*, "Segmentation and Quantification for Angle-Closure Glaucoma Assessment in Anterior Segment OCT," *IEEE Trans Med Imaging*, vol. 36, no. 9, pp. 1930–1938, 2017, doi: 10.1109/TMI.2017.2703147.
4. P. Das, S. R. Nirmala, and J. P. Medhi, "Diagnosis of glaucoma using CDR and NRR area in retina images," *Network Modeling Analysis in Health Informatics and Bioinformatics*, vol. 5, no. 1, p. 3, 2016, doi: 10.1007/s13721-015-0110-5.
5. S. Kavitha, S. Karthikeyan, and K. Duraiswamy, "Neuroretinal rim Quantification in Fundus Images to Detect Glaucoma," *Ijcsns*, vol. 10, no. 6, p. 134, 2010.
6. N. Harizman *et al.*, "The ISNT Rule and Differentiation of Normal From Glaucomatous Eyes," *Arch Ophthalmol.*, vol. 124, no. 11, pp. 1579–1583, 2006.

7. Harini and Sheela, "Feature Extraction and Classification of Retinal Images for Automated Detection of Diabetic Retinopathy," in *2016 Second International Conference on Cognitive Computing and Information Processing (CCIP)*, 2016, pp. 7–10.
8. Y. Dong, Q. Zhang, Z. Qiao, and J. Yang, "Classification of Cataract Fundus Image Based on Deep Learning," in *2017 IEEE International Conference on Imaging Systems and Techniques (IST), Beijing*, 2017, pp. 1–5.
9. S. Choudhury, S. Bandyopadhyay, S. K. Latib, D. K. Kole, and C. Giri, "Fuzzy C Means based Feature Extraction and Classification of Diabetic Retinopathy using Support Vector Machines," in *2016 International Conference on Communication and Signal Processing (ICCSP)*, 2016, pp. 1520–1525.
10. A. Juliansyah and G. S. Nugraha, "Segmentation of Neuro Retinal Rim Area using Histogram Feature-based for Glaucoma Detection in Retinal Fundus Image," in *International Conference on Advanced Computer Science and Information System (ICACSIS) 2019,* 2019, pp. 117–122.
11. J. Sivaswamy, S. R. Krishnadas, and A. Chakravarty, "A Comprehensive Retinal Image Dataset for the Assessment of Glaucoma from the Optic Nerve Head Analysis," *JSM Biomed Imaging Data Pap 2(1): 1004 (2015)*, vol. 2, pp. 1–7, 2015.
12. C. Pena-Betancor *et al*., "Estimation of the relative amount of hemoglobin in the cup and neuro-retinal rim using stereoscopic color fundus images," *IOVS*, p. IOVS–14–15592, 2015.
13. R. Priyadharsini, T. Sree Sharmila, and V. Rajendran, "A wavelet transform based contrast enhancement method for underwater acoustic images," *Multidimens Syst Signal Process*, vol. 29, no. 4, pp. 1845–1859, 2018, doi: 10.1007/s11045-017-0533-5.
14. H. Zeng, L. Li, Z. Cao, and L. Zhang, "Reliable and efficient image cropping: A grid anchor based approach," *Proceedings of the IEEE Computer Society Conference on Computer Vision and Pattern Recognition*, vol. 2019-June, pp. 5942–5950, 2019, doi: 10.1109/CVPR.2019.00610.
15. N. Salem, H. Malik, and A. Shams, "Medical image enhancement based on histogram algorithms," *Procedia Comput Sci*, vol. 163, pp. 300–311, 2019, doi: 10.1016/j.procs.2019.12.112.
16. M. Bohara *et al*., "Histological Grade of Meningioma: Prediction by Intravoxel Incoherent Motion Histogram Parameters," *Acad Radiol*, vol. 27, no. 3, pp. 342–353, 2020, doi: 10.1016/j.acra.2019.04.012.
17. A. Soltani, T. Battikh, I. Jabri, and N. Lakhoua, "A new expert system based on fuzzy logic and image processing algorithms for early glaucoma diagnosis," *Biomed Signal Process Control*, vol. 40, pp. 366–377, 2018.
18. J. E. W. Koh, E. Y. K. Ng, S. v Bhandary, Y. Hagiwara, A. Laude, and U. R. Acharya, "Automated retinal health diagnosis using pyramid histogram of visual words and Fisher vector techniques," *Comput Biol Med*, vol. 92, pp. 204–209, 2018.
19. N. A. Mohamed, M. A. Zulkifley, W. M. D. W. Zaki, and A. Hussain, "An automated glaucoma screening system using cup-to-disc ratio via simple linear iterative clustering superpixel approach," *Biomed Signal Process Control*, vol. 53, p. 101454, 2019.
20. Z. U. Rehman, S. S. Naqvi, T. M. Khan, M. Arsalan, M. A. Khan, and M. A. Khalil, "Multi-parametric optic disc segmentation using superpixel based feature classification," *Expert Syst Appl*, vol. 120, pp. 461–473, 2019.